CHEMISTRY OF MATERIALS

Communication

pubs.acs.org/cm

Single-Crystalline Copper Nano-Octahedra

Shu-Chen Lu,[†] Ming-Cheng Hsiao,[†] Mustafa Yorulmaz,[‡] Lin-Yung Wang,[‡] Po-Yuan Yang,[†] Stephan Link,[‡] Wei-Shun Chang,[‡] and Hsing-Yu Tuan*[,†]

[†]Department of Chemical Engineering, National Tsing Hua University, 101, Section 2, Kuang-Fu Road, Hsinchu, Taiwan 30013, ROC

[‡]Department of Chemistry, Rice University, 6100 Main Street, Houston, Texas 77005, United States

Supporting Information

Coinage nanostructures possess unique optical properties and electric-field enhancements owing to surface plasmon resonances[1] useful for various applications such as sensing,[2] waveguiding,[3] nano-antenna-enhanced spectroscopy.[4] The emerging application of photocatalysis uses the plasmon resonances to generate hot electrons[5] to enhance the catalytic activity of various reactions such as water splitting and hydrogen dissociation.[6,7] The selectivity and reactivity of metal nanocatalysts rely heavily on the facets of the nanoparticles and can be modulated by controlling the morphology of the nanocrystals.[8,9] Cu, compared to Au and Ag, has a larger electron conductivity and higher earth abundance. These properties make Cu attractive as a low-cost plasmonic material. For colloidal solutions, many approaches for tuning the size, shape, and composition of nanoparticles have been developed.[10−12] Nevertheless, few efforts have been made with Cu nanocrystals due to the lack of successful methods for shape control.

Cu nanoparticles are widely used as catalysts for diverse reactions.[13] Although Cu_2O_3 develops on the Cu surface under oxygen exposure, it can be reduced by the clever design of the capping materials[12,14] or depositing a few atomic layers of Al_2O_3.[15] Cu/Au alloy nanoparticles can further passivate Cu from oxidation.[16,17] Furthermore, a recent study showed an active reduction of Cu_2O_3 to Cu by illuminating the Cu nanoparticles with visible light on resonance with the Cu localized surface plasmon resonance (LSPR) and powers larger than 550 mW/cm^2.[18] However, it is difficult to reduce Cu^{II} or Cu^{I} ions to Cu^0 in an aqueous solution, and surface oxidation of Cu tends to occur during reactions. These obstacles have made it difficult to fully develop a synthesis to produce Cu nanoparticles with controllable shapes. Only a few methods could synthesize Cu nanoparticles with controllable shapes and sizes. To date, the most reported example is a Cu nanocube with {100} facets.[19−21] Other shapes remain limited.[12,22−29]

An octahedron with eight {111} facets is regarded as a classic model to study the surface properties of {111} facets. Nonetheless, the precise colloidal synthesis of Cu nano-octahedra has not been reported yet. Herein, we show the successful synthesis of Cu nano-octahedra and investigate their optical properties both experimentally and theoretically. In a typical synthesis of Cu nano-octaheda, precursor solution was prepared by mixing 2 mmol CuCl and 2 mL trioctylphosphine (TOP) in a vial preheated at 200 °C for 2 h. 18 mL of oleylamine (OLA) was added into a three-necked flask and kept under a flow of high-purity argon gas for 40 min with vigorous stirring. After the purge process was completed, OLA was then heated from room temperature to 335 °C before the precursor solution was injected. During the reaction, the color of the solution changed from bright yellow to red-brown, indicating the formation of the Cu nano-octahedra. After centrifugation of the reaction product, the blue color of the supernatant solution indicated unreacted Cu^{II} ions in the liquid and therefore the generation of metallic Cu^0 was via a disproportionation reaction.[19]

Figures 1a and S1 show a large-area scanning electron microscopy (SEM) image of the as-prepared Cu nano-octahedra. The Cu nanoparticles clearly organize into large-scale, regularly ordered patterns with monolayer coverage when the solvent is evaporated in an ambient environment. Figure 1b,c shows partially enlarged SEM images of the as-obtained monolayers of Cu nanoparticles, illustrating that the products are almost all octahedra with an edge length of 145 ± 10 nm. These nanoparticles contact each other by vertices and faces to form a close-packed hexagonal (HCP) array (scheme is shown in Figure 1d). The structure exhibits [111] projection that reveals that nanoparticles sit on the substrate on their {111} facets as the most stable orientation. Figure 1e,f shows large-scale and partially enlarged transmission electron microscopy (TEM) images of the product. More TEM images are shown in Figures S2 and S3. We can see that nano-octahedra form a self-assembled structure on the carbon-coated Cu grid in the same layout as was observed in SEM. Figure 1g is the fast Fourier transformation (FFT) of the region of Figure 1f, revealing HCP packing symmetry. The inset in Figure 1a is a photograph of the as-prepared Cu nano-octahedra in toluene solution (a red-brown color). Figure S4a shows the X-ray diffraction (XRD) pattern recorded from the colloidal products. The only one peak at 43.3° represents the {111} planes (JCPDS card No. 89-2838) in agreement with the face-center cubic (FCC) structure of Cu and explicitly indicates that Cu nanoparticles are highly oriented. The Fourier-transform infrared (FTIR) spectrum of Cu nano-octahedra (Figure S4b) shows symmetric and asymmetric alkane CH_2 stretches at 2848 and 2898 cm^{-1}, respectively, as well as free amines at 3404 cm^{-1}. The NH_2 scissoring peak of OLA is visible at 1626 cm^{-1}. The peak at 1406 cm^{-1} comes from the symmetric rocking mode of the terminal methyl group of TOP, and the C−P stretching peak of

Received: September 9, 2015
Revised: December 3, 2015

DOI: 10.1021/acs.chemmater.5b03519
Chem. Mater. XXXX, XXX, XXX−XXX

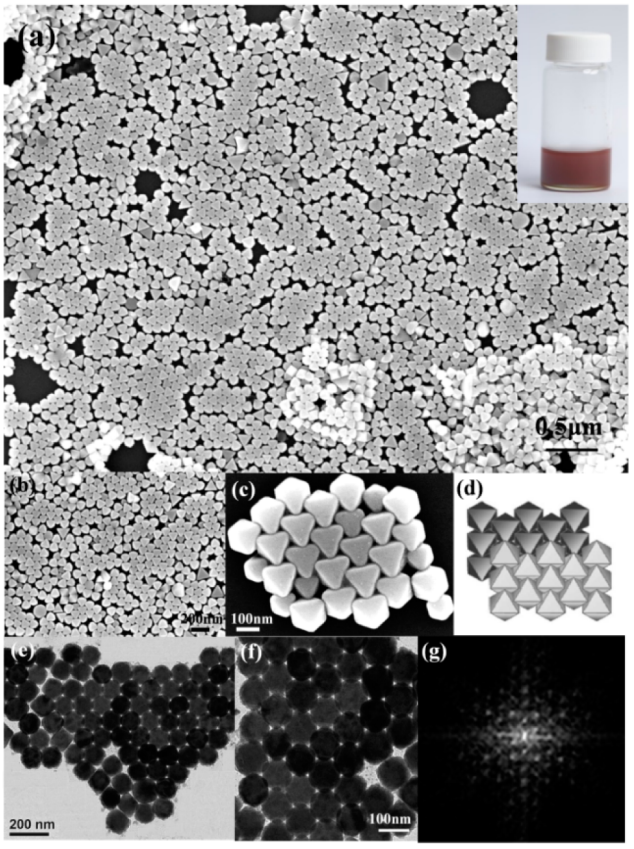

Figure 1. (a) Large-area and (b,c) partially enlarged SEM images of the as-prepared Cu nano-octahedra with an average size of 145 ± 10 nm. (d) Scheme of the Cu nano-octahedra self-assembled into a HCP array. (e) Large-scale and (f) partially enlarged TEM images of the Cu nano-octahedra. (g) FFT of the TEM image in (f). The insert in panel a is a photo of the as-synthesized Cu nano-octahedra in toluene solution.

TOP is seen at 1082 cm^{-1}. These results indicate that TOP molecules on the surface of Cu nanoparticles may lead to their octahedral shape. The X-ray photoelectron spectrum (XPS) of Cu nano-octahedra (Figure S4c,d) shows the main peaks of Cu $2p_{3/2}$ and Cu $2p_{1/2}$ located at 932.2 and 952 eV, respectively, originating from Cu^0 species. The P 2p peak also appears in the XPS spectrum, but disappears after ozone plasma cleaning of the sample. This result indicates that TOP molecules just attach on the surface of these Cu particles (Figure S4d).

Figure 2a–c shows SEM images of different orientations of octahedral particles observed from various projection axes. An octahedron exhibits three different projected shapes: a hexagon (Figure 2d), a rectangle (Figure 2e), and a rhombus (Figure 2f) when viewed along [111], [112], and [110] axes, respectively.[30] For example, an octahedron lying on a planar surface against one of its faces instead of an edge or a corner yields a hexagonal projected shape, as shown in Figure 2f, confirming that the Cu nano-octahedron is bounded by {111} planes. Figure 2g–i display the selected area electron diffraction (SAED) pattern of the corresponding Cu octahedral nanoparticles of Figure 2d–f. A hexagonal shape converts to a rectangular shape after tilting by 19.5 degrees which matches with the change of an octahedron tilted by the same degree (Figure S5). The dark-field image of a single particle using a {111} reflected beam shows the bound (111) plane (Figure S6). A high-magnification TEM image taken from a single octahedron

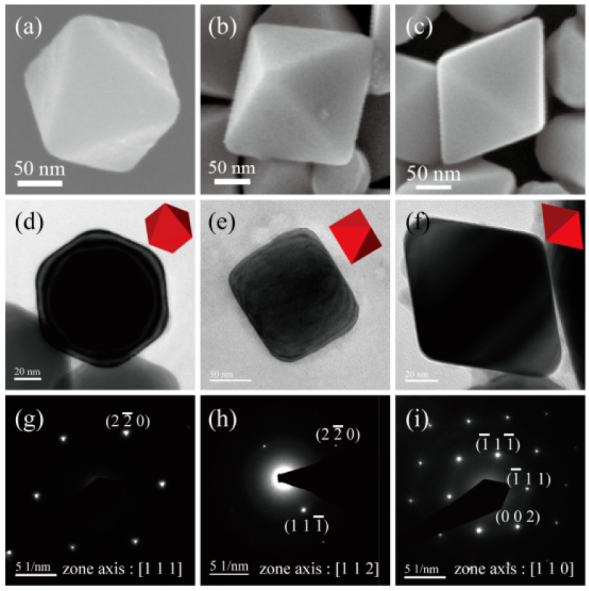

Figure 2. (a–c) SEM images of different orientations of a Cu octahedron. (d–f) TEM images of a Cu octahedron viewed from [111], [112], and [110] axes, respectively. Insets: corresponding schematics for panels a–c. (g–i) SAED patterns of corresponding Cu octahedra shown in panels d–f.

(Figure S7) indicates a single crystalline structure with well-defined fringes. The lattice spacing of the nano-octahedron is 0.21 nm, in agreement with the {111} lattice spacing of FCC Cu.

Noble metal (Cu, Ag, Au) nanoparticles exhibit unique optical properties in the visible and near-infrared regions owing to the LSPR.[31,32] Due to the lossy nature of the metal, the LSPR is inevitably damped by the interband transition.[33] The onset of the interband transition of Cu, Ag, and Au are ~2.1, 3.8, and 2.5 eV, respectively.[34] Ag nanoparticles show stronger LSPR responses as the plasmon peak is shifted farther from the interband transition while the plasmon band of most Cu nanoparticles is much less pronounced because of the overlap of the LSPR band with the interband transition. Hence, it is desirable to synthesize Cu nanoparticles with the plasmon band shifted away from the interband transition.[12,34] The ensemble extinction spectrum of the Cu nano-octahedra in toluene as measured by UV–vis spectroscopy is shown in Figure 3a. Two peaks at 670 and 1120 nm, energetically below the interband transition of Cu (590 nm), were observed. To identify the origin of these peaks, single-particle scattering spectroscopy correlated with high resolution SEM imaging and finite difference time domain (FDTD) simulations were performed (see Supporting Information for experimental and simulation details). Figure 3b shows a scattering spectrum of a single Cu nano-octahedron with an edge size of 155 nm (inset of Figure 3b) on an ITO glass substrate. A single peak at ~650 nm agrees well with the FDTD simulation using identical dimensions as the experimental geometry (Figure 3c). The measured scattering spectra of an additional 6 nanoparticles are shown in Figure S8. These results verify that the peak at 670 nm in the ensemble spectrum originates from single octahedra. Unlike the LSPR band of the small Cu nanoparticles, the plasmon band of Cu nano-ochehedra in this study peaked at 670 nm red-shifted from the interband transition, mostly arising from the larger size of the nanoparticles. The blue-shift of the single-particle scattering spectrum compared to the ensemble measurement

DOI: 10.1021/acs.chemmater.5b03519
Chem. Mater. XXXX, XXX, XXX–XXX

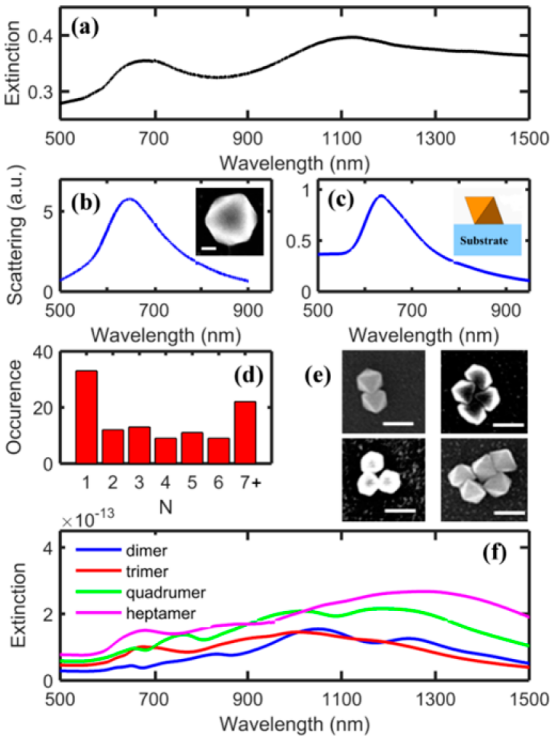

Figure 3. (a) Ensemble extinction spectrum of Cu nano-octahedra in toluene solution. (b) Measured and (c) simulated scattering spectra of a single Cu nano-octahedron. The correlated SEM image and simulation condition are shown in the insets of (b) and (c), respectively. The scale bar represents 50 nm. (d) Histogram of aggregate size expressed as the number of particles per nano-object for a sample span-cast on a Si wafer. (e) SEM images of a dimer, trimer, quadrumer, and heptamer. The scale bar represents 200 nm. (f) Simulated extinction spectra of a dimer, trimer, quadrumer, and heptamer in toluene.

arises from the refractive index of the surrounding media (n = 1.25 the average of air and glass vs n = 1.496 in toluene).

The broad peak at 1120 nm originates from the aggregation of the nano-octahedra. To verify the conformation of the aggregates, an as-prepared solution was spun-cast on a silicon wafer to avoid further aggregation during the evaporation of the solvent. SEM images of ∼100 nanoparticles were recorded to identify the number of nanoparticles per individual aggregate. The histogram in Figure 3d shows a broad distribution of the particle number per aggregate despite the fact that isolated single particles dominate the distribution. SEM images of representative aggregates consisting of 2−5 nanoparticles are shown in Figure 3e. Figure 3f displays the corresponding extinction spectra calculated by the FDTD method based on the geometry obtained via SEM. The simulated spectra show broad peaks around 1000−1300 nm, consistent with the broad peak at 1120 nm observed in the ensemble spectrum. The details of the simulation conditions are shown in Figure S9.

In summary, single-crystalline Cu nano-octahedra with well-defined edge lengths were synthesized successfully via a hot-injection method using TOP as capping ligand. The nano-octahedra tend to self-assemble into HCP arrays and their assembled structure is here confirmed via SEM and TEM. Furthermore, the optical properties of as-prepared Cu nano-octahedra were investigated both experimentally and theoretically.

■ ASSOCIATED CONTENT

Supporting Information

The Supporting Information is available free of charge on the ACS Publications website at DOI: 10.1021/acs.chemmater.5b03519.

Experimental and simulation details, SEM images, TEM images, XRD pattern, FTIR spectra, XPS spectra, dark-field images, and scattering spectra of Cu nano-octahedra (PDF).

■ AUTHOR INFORMATION

Corresponding Author

*H.-Y. Tuan. E-mail: hytuan@che.nthu.edu.tw.

Notes

The authors declare no competing financial interest.

■ ACKNOWLEDGMENTS

H.-Y. T acknowledges the financial support by the (NSC 102-2221-E-007-023-MY3, MOST 103-2221-E-007-089-MY3), sing-Hua University, MOST 103-2622-E-007-025, and MOST 102-2633-M-007-002). S.L. acknowledges financial support from the Robert A. Welch Foundation (C-1664), the Army Research Office (MURI W911NF-12-1-0407), and the Air Force Office of Scientific Research (MURI FA9550-15-1-0022). M.Y. acknowledges financial support from the Smalley Curl Institute at Rice University through a Carl&Lillian Illig Postdoctoral Fellowship. We thank Dr. Jana Olson for editing this paper.

■ REFERENCES

(1) Xia, Y.; Xiong, Y.; Lim, B.; Skrabalak, S. E. Shape-Controlled Synthesis of Metal Nanocrystals: Simple Chemistry Meets Complex Physics? *Angew. Chem., Int. Ed.* **2009**, *48*, 60.

(2) Mayer, K. M.; Hafner, J. H. Localized Surface Plasmon Resonance Sensors. *Chem. Rev.* **2011**, *111*, 3828.

(3) Lal, S.; Hafner, J. H.; Halas, N. J.; Link, S.; Nordlander, P. Noble Metal Nanowires: From Plasmon Waveguides to Passive and Active Devices. *Acc. Chem. Res.* **2012**, *45*, 1887.

(4) Atwater, H. A.; Polman, A. Plasmonics for improved photovoltaic devices. *Nat. Mater.* **2010**, *9*, 205.

(5) Brongersma, M. L.; Halas, N. J.; Nordlander, P. Plasmon-induced hot carrier science and technology. *Nat. Nanotechnol.* **2015**, *10*, 25.

(6) Mubeen, S.; Lee, J.; Singh, N.; Kramer, S.; Stucky, G. D.; Moskovits, M. An Autonomous Photosynthetic Device in which All Charge Carriers Derive from Surface Plasmons. *Nat. Nanotechnol.* **2013**, *8*, 247.

(7) Mukherjee, S.; Libisch, F.; Large, N.; Neumann, O.; Brown, L. V.; Cheng, J.; Lassiter, J. B.; Carter, E. A.; Nordlander, P.; Halas, N. J. Hot Electrons Do the Impossible: Plasmon-Induced Dissociation of H2 on Au. *Nano Lett.* **2013**, *13*, 240.

(8) Jakdetchai, O.; Nakajima, T. Mechanism of the water−gas shift reaction over Cu(110), Cu(111) and Cu(100) surfaces: an AM1-d study. *J. Mol. Struct.: THEOCHEM* **2002**, *619*, 51.

(9) Leng, M.; Liu, M.; Zhang, Y.; Wang, Z.; Yu, C.; Yang, X.; Zhang, H.; Wang, C. Polyhedral 50-Facet Cu2O Microcrystals Partially Enclosed by {311} High-Index Planes: Synthesis and Enhanced Catalytic CO Oxidation Activity. *J. Am. Chem. Soc.* **2010**, *132*, 17084.

(10) Lu, X.; Rycenga, M.; Skrabalak, S. E.; Wiley, B.; Xia, Y. Chemical Synthesis of Novel Plasmonic Nanoparticles. *Annu. Rev. Phys. Chem.* **2009**, *60*, 167.

(11) Eustis, S.; El-Sayed, M. A. Why gold nanoparticles are more precious than pretty gold: Noble metal surface plasmon resonance and its enhancement of the radiative and nonradiative properties of nanocrystals of different shapes. *Chem. Soc. Rev.* **2006**, *35*, 209.

DOI: 10.1021/acs.chemmater.5b03519
Chem. Mater. XXXX, XXX, XXX−XXX

(12) Pastoriza-Santos, I.; Sánchez-Iglesias, A.; Rodríguez-González, B.; Liz-Marzán, L. M. Aerobic Synthesis of Cu Nanoplates with Intense Plasmon Resonances. *Small* **2009**, *5*, 440.
(13) Son, S. U.; Park, I. K.; Park, J.; Hyeon, T. Synthesis of Cu2O coated Cu nanoparticles and their successful applications to Ullmann-type amination coupling reactions of aryl chlorides. *Chem. Commun.* **2004**, 778.
(14) Chen, C.; Ahmed, I.; Fruk, L. Reactive oxygen species production by catechol stabilized copper nanoparticles. *Nanoscale* **2013**, *5*, 11610.
(15) Sun, Q.-C.; Ding, Y.; Goodman, S. M.; H. Funke, H.; Nagpal, P. Copper plasmonics and catalysis: role of electron-phonon interactions in dephasing localized surface plasmons. *Nanoscale* **2014**, *6*, 12450.
(16) Chen, S.; Jenkins, S. V.; Tao, J.; Zhu, Y.; Chen, J. Anisotropic Seeded Growth of Cu−M (M = Au, Pt, or Pd) Bimetallic Nanorods with Tunable Optical and Catalytic Properties. *J. Phys. Chem. C* **2013**, *117*, 8924.
(17) He, R.; Wang, Y.-C.; Wang, X.; Wang, Z.; Liu, G.; Zhou, W.; Wen, L.; Li, Q.; Wang, X.; Chen, X.; Zeng, J.; Hou, J. G. Facile synthesis of pentacle gold−copper alloy nanocrystals and their plasmonic and catalytic properties. *Nat. Commun.* **2014**, *5*, 4327.
(18) Marimuthu, A.; Zhang, J.; Linic, S. Tuning Selectivity in Propylene Epoxidation by Plasmon Mediated Photo-Switching of Cu Oxidation State. *Science* **2013**, *339*, 1590.
(19) Guo, H.; Liu, X.; Xie, Q.; Wang, L.; Peng, D.-L; Branco, P. S.; Gawande, M. B. Disproportionation route to monodispersed copper nanoparticles for the catalytic synthesis of propargylamines. *RSC Adv.* **2013**, *3*, 19812.
(20) Guo, H.; Chen, Y.; Cortie, M. B.; Liu, X.; Xie, Q.; Wang, X.; Peng, D.-L. Shape-Selective Formation of Monodisperse Copper Nanospheres and Nanocubes via Disproportionation Reaction Route and Their Optical Properties. *J. Phys. Chem. C* **2014**, *118*, 9801.
(21) Yang, H.-J.; He, S.-Y.; Chen, H.-L.; Tuan, H.-Y. Monodisperse Copper Nanocubes: Synthesis, Self-Assembly, and Large-Area Dense-Packed Films. *Chem. Mater.* **2014**, *26*, 1785.
(22) Guo, H.; Chen, Y.; Ping, H.; Jin, J.; Peng, D.-L. Facile Synthesis of Cu and Cu@Cu-Ni Nanocubes and Nanowires in Hydrophobic Solution in the Presence of Nickel and Chloride Ions. *Nanoscale* **2013**, *5*, 2394.
(23) Guo, H. Z.; Lin, N.; Chen, Y. Z.; Wang, Z. W.; Xie, Q. S.; Zheng, T. C.; Gao, N.; Li, S. P.; Kang, J. Y.; Cai, D. J.; Peng, D. L. Copper Nanowire as Fully Transparent Conductive Electrodes. *Sci. Rep.* **2013**, *3*, 2323.
(24) Wang, Y.; Chen, P.; Liu, M. Synthesis of well-definced copper nanocubes by a one-pot solution process. *Nanotechnology* **2006**, *17*, 6000.
(25) Xiao, B.; Niu, Z.; Wang, Y.-G.; Jia, W.; Shang, J.; Zhang, L.; Wang, D.; Fu, Y.; Zeng, J.; He, W.; Wu, K.; Li, J.; Yang, J.; Liu, L.; Li, Y. Copper Nanocrystal Plane Effect on Stereoselectivity of Catalytic Deoxygenation of Aromatic Epoxides. *J. Am. Chem. Soc.* **2015**, *137*, 3791.
(26) Xu, R.; Xie, T.; Zhao, Y. G.; Li, Y. D. Single-Crystal Metal nanoplatelets: Cobalt, Nickel, Copper, and Silver. *Cryst. Growth Des.* **2007**, *7*, 1904.
(27) Ko, W.-Y.; Chen, W.-H.; Tzeng, S.-D.; Gwo, S.; Lin, K.-J. Synthesis of Pyramidal Copper Nanoparticles on Gold Substrate. *Chem. Mater.* **2006**, *18*, 6097.
(28) Tanori, J.; Pileni, M. P. Control of the Shape of Copper Metallic Particles by Using a Colloidal System as Template. *Langmuir* **1997**, *13*, 639.
(29) Yang, H.-J.; He, S.-Y.; Tuan, H.-Y. Self-Seeded Growth of Five-Fold Twinned Copper Nanowires: Mechanistic Study, Characterization, and SERS Applications. *Langmuir* **2014**, *30*, 602.
(30) Guo, H.; Chen, Y.; Ping, H.; Wang, L.; Peng, D.-L. J. Mater. Chem. One-pot synthesis of hexagonal and triangular nickel-copper alloy nanoplates and their magnetic and catalytic properties. *J. Mater. Chem.* **2012**, *22*, 8336.
(31) Quan, Z.; Fang, J. Superlattices with non-spherical building blocks. *Nano Today* **2010**, *5*, 390.
(32) West, P. R.; Ishii, S.; Naik, G. V.; Emani, N. K.; Shalaev, V. M.; Boltasseva, A. Searching for better plasmonic materials. *Laser Photon. Rev.* **2010**, *4*, 795.
(33) Boltasseva, A.; Atwater, H. A. Low-Loss Plasmonic Metamaterials. *Science* **2011**, *331*, 290.
(34) Wang, H.; Tam, F.; Grady, N. K.; Halas, N. J. Cu Nanoshells: Effects of Interband Transitions on the Nanoparticle Plasmon Resonance. *J. Phys. Chem. B* **2005**, *109*, 18218.

DOI: 10.1021/acs.chemmater.5b03519
Chem. Mater. XXXX, XXX, XXX−XXX